

Disk Substructures at High Angular Resolution Program (DHARP):  
X. Multiple ring-structure in AS209 [Ideas for a better title are welcome]

V. V. GUZMÁN<sup>1</sup> AND ET AL.<sup>2, 3, 4, 5</sup>

<sup>1</sup>*Joint ALMA Observatory*

<sup>2</sup>*Harvard-Smithsonian Center for Astrophysics, 60 Garden Street, Cambridge, MA 02138, USA*

<sup>3</sup>*Rice University USA*

<sup>4</sup>*Universidad de Chile*

<sup>5</sup>*Others*

## ABSTRACT

We present high-angular resolution observations of the 1.2 mm continuum and  $^{12}\text{CO}$  2 – 1 emission from the disk around the T Tauri star AS 209. The dust emission consists of a series of packed rings in the inner  $\sim 60$  au disk, and two bright disks in the outer disk, centered at 74 and 120 au. The gap between the two outer rings is not completely empty, as some faint emission is detected. We also find an additional faint emission bump in the outer disk, extending out to 160 au. We modeled the surface brightness emission in the uv-plane and are able reproduce the observations with a simple model of 8 concentric Gaussian rings. Some low level residuals in the inner disk, however, hint at a slightly different inclination for the rings in the inner disk compared to the rings in the outer disk. The  $^{12}\text{CO}$  line emission is centrally peaked, although it presents substructure, and extends out to  $\sim 300$  au, much farther out than the millimeter dust emission. We find CO depletion at four radii in the outer disk, near 45, 75, 120 and 210 au. The outermost gap is located well beyond the edge of the millimeter dust emission, and thus cannot be due to dust opacity and must be caused by a real depletion in the CO abundance due to a chemical effect or by a total gas depletion.

*Keywords:* circumstellar matter — planetary systems: formation, protoplanetary disks — dust

## 1. INTRODUCTION

The distribution of gas and dust in protoplanetary disks will impact directly the outcome of planetary systems (Öberg et al. 2011). Characterizing the spatial distribution of both the dust and a gas in disks is therefore essential to understand how and what kind of planets can form. The main problem theoretical models currently have is the fast migration of mm-sized dust particles towards the central star, preventing the formation of planetesimals, specially at larger distances from the star. The solution that has been invoked to solve this problem is the presence of local pressure maxima that can stop, at least temporarily, the migration of solid particles and concentrate them for enough time to allow them to grow and form larger bodies (e.g., Pinilla et al. 2012). In the recent years, high-angular resolution ALMA observations of the dust continuum emission have shown evidence of such substructures in a handful of disks around nearby young stars, namely HL Tau (ALMA Partnership et al. 2015), HD 163296 (Isella et al. 2016), and AS 209 Fedele et al. (2018), Elias 2-24 (Cieza et al. 2017) and even in the older TW Hya disk (Andrews et al. 2016). All of these disks present multiple ring/gap structures, and demonstrate the presence of mm-sized grains in the outer disk. The origin of these ring-like substructures is unclear. The most favored mechanisms include planet-disk interactions (e.g. Dong & Fung 2017), radial pressure variations due to zonal flows in MHD turbulent disks (Johansen et al. 2009), and snowline-induced gaps (Zhang et al. 2015).

While the presence of substructures seems universal, a larger sample of disks is needed to fully characterize the prevalence and configuration of such substructures, and constrain the physical or chemical process responsible for them. This is the motivation of The Disk Substructures at High Angular Resolution Project (DSHARP), one of the Large Program carried out with the Atacama Large Millimeter Array (ALMA). The goal of the project is to characterize in an homogeneous way the substructures of 20 nearby protoplanetary disks, by mapping the 240 GHz dust continuum emission at a resolution of 35 mas, corresponding to 5 au, on average (Andrews et al. 2018). One of the main outcomes of this survey is that that rings and gaps are an extremely common feature of disks, but the configuration (position and contrast) of the rings varies substantially from source to source (Huang et al. 2018a).

In this paper we focus on one the DSHARP sources, the disk around the classical T Tauri AS 209 star. The star is located in the Ophiuchus star forming region, at a

distance of  $121 \pm 2$  pc (Gaia Collaboration et al. 2018), although it is relatively isolated from the main cloud. The star has a spectral type K5, a mass of  $0.9 M_{\odot}$ , and is 1.6 Myr old (Herbig & Bell 1988). Observations at different wavelengths clearly show the effect of radial drift of larger grains, as the emission is noticeably more compact at longer wavelengths (Pérez et al. 2012; Tazzari et al. 2016). The surface density profile has been characterized with  $870 \mu\text{m}$  observations at  $0.3''$  angular resolution (Andrews et al. 2009). More recently, Fedele et al. (2018) presented ALMA observations of the disk at  $\sim 0.15''$  angular resolution. The emission was characterized by a bright central component and the presence of two weaker dust rings near 75 and 130 au, and two gaps near 62 and 103 au. No obvious substructure was observed in the inner 60 au disk, except for a kink around 20 – 30 au. Fedele et al. (2018) also presented hydro-dynamical simulations and found that the gap near 100 au located between the two outer rings could be produced by a Saturn-like planet.

Observations of the scattered light emission from the AS 209 disk have been recently presented by Avenhaus et al. (2018). The emission is surprisingly faint and compact compared to other disks of similar dust mass and age. Moreover, AS 209 presents a large IR excess, which usually results in bright scattered light emission. This could be the result of self-shadowing of the inner disk, although the most likely alternative is that the disk is very settled which hampers the efficient scattering of photons from the star.

The disk has also been observed in molecular line emission. Huang et al. (2016) presented observations of the three CO isotopologues at  $0.6''$  angular resolution. While the emission from the most abundant isotopologue,  $^{12}\text{CO}$ , was found to be centrally peaked and decreasing monotonically with radius, the  $^{13}\text{CO}$  and  $\text{C}^{18}\text{O}$  emission showed evidence of an outer ring or bump centered at 150 au, near the millimeter dust edge.

In this paper we present 1.2 mm dust continuum and  $^{12}\text{CO}$  2 – 1 line observations in the AS 209 disk. The observations and data reduction are presented in section 2. The results of the dust continuum emission and the  $^{12}\text{CO}$  line emission are described in section 3. A discussion is presented in section 4 and a summary is given in section 5.

## 2. OBSERVATIONS

The observations presented here are part of the DSHARP ALMA Large Program (2016.1.00484.L). The AS 209 disk was observed with ALMA in Band 6 in September 2017 in configurations C40-8/9. Shorter-baselines were observed in May 2017 in configuration C40-5. We use additional archival data from projects 2013.1.00226 (Huang et al. 2016) and 2015.1.00486.S (Fedele et al. 2018), that provide information on shorter and intermediate baselines, respectively.

A detailed description of the observations and data reduction process can be found in Andrews et al. (2018). Briefly, we first self-calibrated the short baselines, and in a second step self-calibrated the combined observations of short- and long-baselines. The observations were cleaned in CASA 5.1, using the multi-scale option and a robust parameter of 0. The resulting image has a beam of  $0.04'' \times 0.03''$ , position angle of  $-81^\circ$  and a rms noise of  $1.5 \mu\text{Jy beam}^{-1}$ .

The solutions of the self-calibration of the continuum emission were then applied to the  $^{12}\text{CO}$  data. The molecular line data was first regridded to channels of  $0.35 \text{ km s}^{-1}$  and then cleaned with a robust parameter of 1.0. A Keplerian mask was used to help the cleaning process. We set the deconvolver parameter to *multiscale* in tclean, with scales 0, 10, 25, 75, 150 and 250. The resulting image has a beam of  $0.09'' \times 0.07''$ , position angle of  $-83^\circ$  and a rms noise of  $0.77 \text{ mJy beam}^{-1}$  per channel.

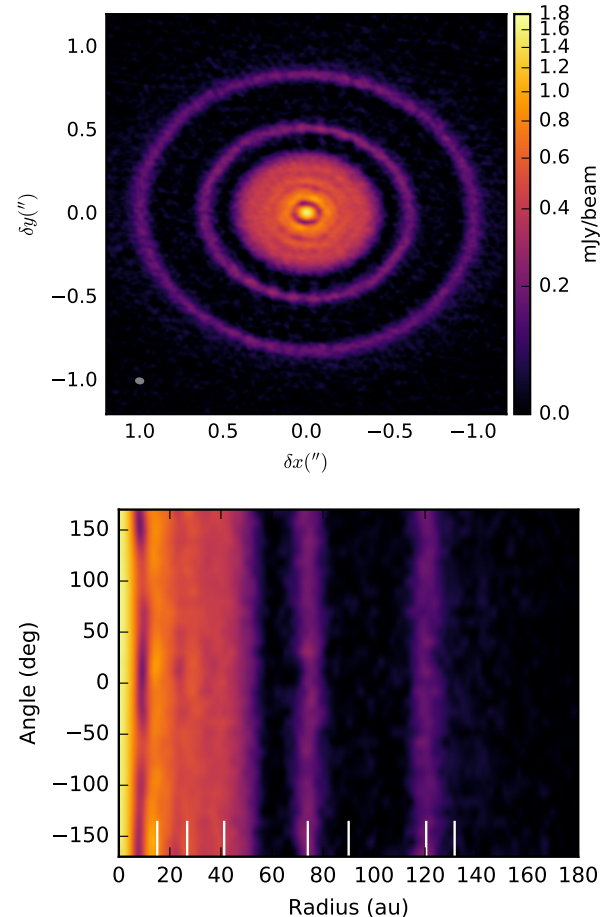


**Figure 1.** The dust continuum emission map (upper panel), and the deprojected emission shown in polar coordinates (bottom panel). The beam of  $0.03'' \times 0.04''$  is shown in the bottom left, corresponding to a spatial resolution of  $3.6 \times 4.8$  au.

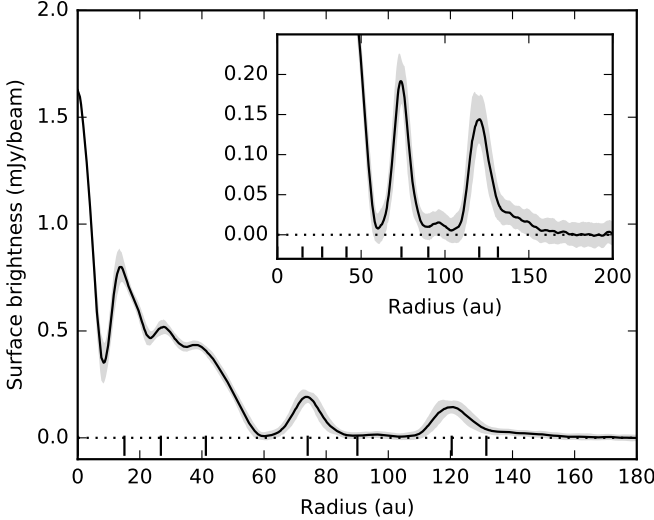


**Figure 2.** Deprojected azimuthally-averaged radial profile of the dust continuum emission. The gray ribbon shows the standard deviation at each radius, and the vertical bars show the location of the rings given by our best-fit model.

### 3. RESULTS

In this section we first describe the main features of the dust continuum emission and model the surface brightness in the uv-plane to extract the position and width of the different ring components. We then describe the spatial distribution of the  $^{12}\text{CO}$  emission and its relation to the dust continuum emission.

#### 3.1. Dust continuum emission

The map of the 1.2 mm dust continuum emission from the AS 209 disk is shown in Fig. 1. The map is shown in the upper panel with the beam size in the bottom left corner. The lower panel shows the emission in polar coordinates, to better visualize the axisymmetric nature of the emission. The dust emission is characterized by a series of concentric narrow rings and gaps. Fig. 2 shows the deprojected azimuthally averaged emission profile, assuming an inclination of  $35^\circ$  and position angle of  $86^\circ$  for the disk (see section 3.1.1). The emission is centrally peaked and the surface brightness of the rings decreases with radius. A striking aspect of the emission is the difference between the inner  $< 60$  au disk, that consists of several closely packed rings, and the outer  $> 60$  au disk that consists of 2 bright rings that are well separated and spatially resolved. The two outer rings have been previously reported by Fedele et al. (2018). The new higher-angular resolution observations reveal the inner disk is not smooth but contains substantial substructure. The rings in the inner disk are blended but spatially resolved by our beam. The gap near 100 au is not completely empty of emission, as a bump can be seen in the deprojected radial profile around this radius (better seen in the zoomed panel in Fig. 2). An additional faint

component can also be seen at the edge of the disk, just outside the bright ring located at  $\sim 120$  au.

In the next section, we model the emission in the uv-plane to obtain the beam-corrected position and width of the various rings observed in the disk.

#### 3.1.1. Model-fitting in the uv-plane

Given the striking ring-nature of the dust continuum emission, we modeled the radial brightness distribution with the sum of concentric Gaussian rings:

$$I(r) = \sum_{i=0}^N A_i \exp(-(r - r_i)^2 / 2\sigma_i^2). \quad (1)$$

The number of rings is chosen by a first eye-examination of the cleaned emission map and the deprojected radial profile (see Figs. 1 and 2). We include 4 rings in the inner ( $< 60$  au) disk and 4 rings in the outer disk. The position of the innermost Gaussian is fixed to zero, i.e., the disk center. Two of outer rings correspond to the faint components near 100 and 140 au. We assume the emission is symmetric, and create synthetic visibilities given by the Henkel transform (Pearson 1999):

$$V(\rho) = 2\pi \int_0^\infty I_\nu(r) J_0(2\pi\rho r) r dr \quad (2)$$

where  $\rho$  is the deprojected uv-distance in units of  $k\lambda$ ,  $r$  is the radial angular distance from the disk center in units of radians, and  $J_0$  is the zeroth-order Bessel function of the first kind.

The observed visibilities are first deprojected, radially averaged and binned. We include uv-points from

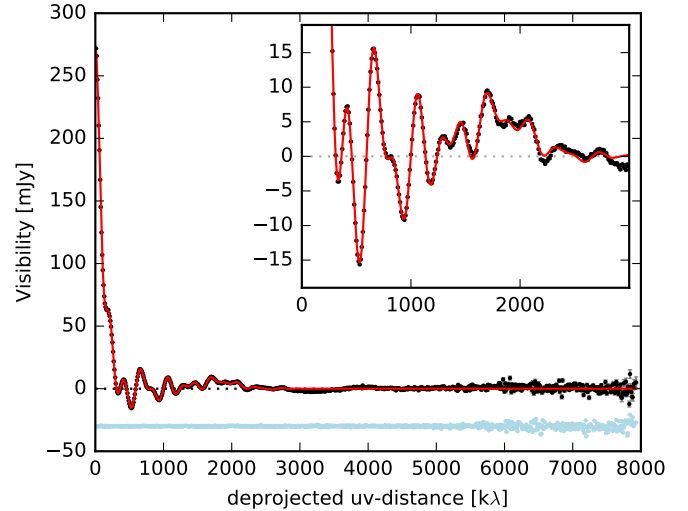


**Figure 3.** Observed (black) and best-fit model (red) deprojected visibilities. The imaginary part of the observed visibilities are shown in light-blue (shifted to  $-30$  mJy). We only fit  $u - v$  distances  $< 3000$   $k\lambda$ , and assume the emission is axisymmetric.

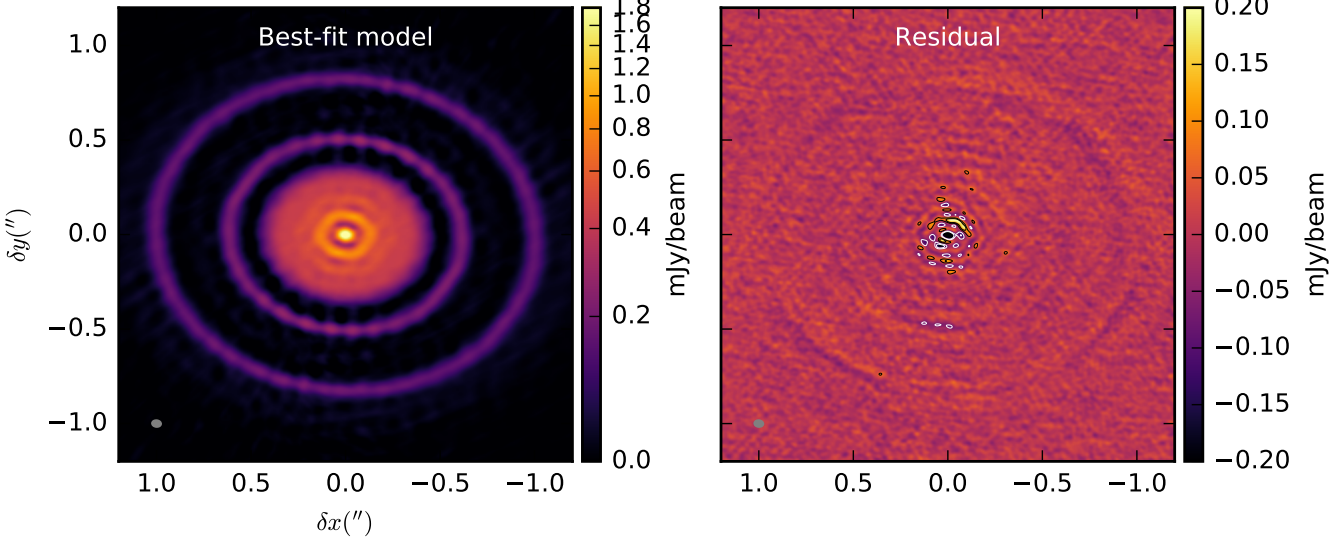


**Figure 4.** Best-fit model (left) and residual (right) maps. The residuals are shown in linear scale, and contours of 5 and  $10 \times$  the rms noise are drawn in white and black, for positive and negative residuals, respectively.

10 to 10000  $k\lambda$ , in steps of 10  $k\lambda$ . To speed-up the fitting method, we only fit visibilities with uv-distances  $< 3000 k\lambda$ . The inclination ( $i$ ), position angle (PA) and center of the disk, given by an offset ( $\delta_x$ ,  $\delta_y$ ), are included as free parameters in the fit. The total number of free parameters is then 27, that is 23 for the Gaussian rings ( $A_i, r_i, \sigma_i$  with  $i$  from 1 to 8;  $r_0 = 0$ ) and 4 for the disk geometry ( $i$ , PA,  $\delta_x$ ,  $\delta_y$ ).

We use the `emcee` package (Foreman-Mackey et al. 2013), which is an implementation of the MCMC method, to sample the posterior distribution and explore the parameter space. Table 1 summarizes the resulting best-fit parameters.

We find a disk inclination of  $34.9^\circ$  and a position angle of  $85.5^\circ$ , which are consistent with previous estimates (Fedele et al. 2018). We also find a small offset from the phase center. The four rings in the inner disk are located at 0, 15, 27, 41 au, and have FWHM between 7 and 17 au. The two prominent rings in the outer disk are centered at 74 and 120 au. Fedele et al. (2018) found this second ring to be located at 130 au instead of 120 au. The difference is due to the presence of another much fainter ring or bump, which we find to be centered at 132 au. The faint ring located in between the two prominent outer rings is centered at 90 au. We note that this ring is not located at the gap center but is instead close to the inner ring near 74 au. Also, the two faint rings in the outer disk are found to be much broader (FWHM of 19 and 36 au) than the rest of the rings, in particular the two prominent outer rings which have FWHM of  $\sim 8$  au. This suggest that these components are not proper rings and are thus not well represented by a Gaussian, and could instead be treated as faint emission

that is somehow connected to their brighter neighbor rings.

Fig. 3 shows the observed real part of the deprojected visibilities in black, using the best-fit disk inclination and position angle. The imaginary part of the visibilities are shown in light-blue (shifted by  $-30$  mJy), and remain close to zero for all uv-distance, consistent with symmetric emission of the disk. A zoom of the  $< 3000 k\lambda$  visibilities is shown in the upper-right panel of the figure. Our simple parametric model of pure Gaussian rings can recover most of the (very complicated) structure seen in the radially averaged visibility profile. The cleaned image of the best-fit model is shown in Fig. 4. The residuals, corresponding to the cleaned

**Table 1.** Best-fit parameters.

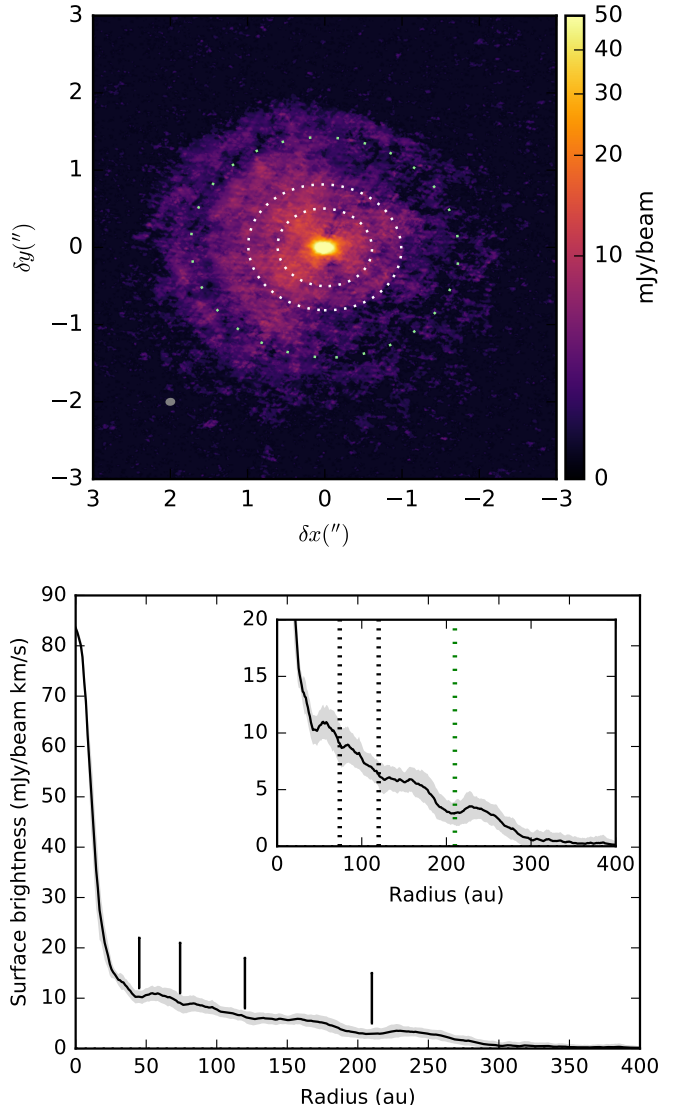
Disk geometry			
$i$ (deg)	PA (deg)	$\delta_x$ (mas)	$\delta_y$ (mas)
$34.887_{-0.0023}^{+0.0014}$	$85.453_{-0.0029}^{+0.0045}$	$1.617_{-0.0984}^{+0.0389}$	$-3.143_{-0.0088}^{+0.0173}$
Gaussian Rings			
Ring	Rel. Amp	$r_i$ (au)	FWHM (au)
1	$1.000_{-0.0065}^{+0.0061}$	0.00	$6.64_{-0.02}^{+0.03}$
2	$0.270_{-0.0006}^{+0.0007}$	$15.03_{-0.01}^{+0.02}$	$7.18_{-0.04}^{+0.04}$
3	$0.133_{-0.0005}^{+0.0004}$	$26.79_{-0.03}^{+0.03}$	$11.76_{-0.11}^{+0.13}$
4	$0.114_{-0.0003}^{+0.0003}$	$41.38_{-0.05}^{+0.06}$	$17.35_{-0.08}^{+0.07}$
5	$0.074_{-0.0003}^{+0.0003}$	$74.04_{-0.01}^{+0.01}$	$7.23_{-0.04}^{+0.03}$
6	$0.004_{-0.0001}^{+0.0001}$	$90.04_{-0.03}^{+0.07}$	$19.12_{-0.30}^{+0.26}$
7	$0.048_{-0.0001}^{+0.0002}$	$120.42_{-0.01}^{+0.01}$	$8.26_{-0.04}^{+0.05}$
8	$0.009_{-0.0001}^{+0.0000}$	$131.74_{-0.13}^{+0.13}$	$35.72_{-0.17}^{+0.17}$

image of residual visibilities ( $V_{obs} - V_{model}$ ) are shown in the right panel of the figure. Our best-fit model successfully reproduces the observations, as seen by the low-level emission in the residuals map. However, an asymmetry is seen in the residuals map near the disk center, which suggests that the rings in the inner  $\sim 10$  au disk have a slightly different orientation than the rest of the disk.

### 3.2. CO emission

Figure 5 shows the moment-zero map of the CO 2 – 1 line, integrated from  $-3$  to  $14$  km s $^{-1}$ . Pixels with S/N ratio lower than 3 have been clipped to highlight the substructure of the emission. The West side of the disk is heavily affected by cloud contamination, which explains the East-West asymmetry of the emission in the disk. The bottom panel in Fig. 5 displays the azimuthally-averaged deprojected profile, including only the East side of the disk. A selection of channels, showing the emission from the East-side of the disk is shown in Fig. 6. Channel maps for the full velocity range can be found in Fig. 7. The CO emission is 1) centrally peaked, 2) extends much farther out than the millimeter dust emission (out to 300 au), and 3) presents 4 main gaps or decrease of emission in the outer disk, near 45, 75, 120 and 210 au. We note this is not an effect of the clipping in the creation the moment-zero map, as the gaps are also seen with even more clarity in the individual channels (see Fig. 6). The first gap is located very close to the edge of the inner millimeter disk. The next two gaps or CO depletions near 74 and 120 au spatially coincides the two prominent outer dust ring. This gap is better seen in the channel maps, at a velocity of 5.8 km s $^{-1}$ . The spatial coincidence of these two gaps with the location of the millimeter dust rings suggest that the rings are optically thick and are absorbing the CO emission (see the discussion in section 4.2). The fourth and outermost gap seen in the CO emission is located at a distance of 210 au from the central star, well beyond the millimeter dust edge. Therefore, it cannot be explained by dust opacity and must be a real decrease in the abundance of gaseous CO or a substantial reduction of the gas density at this radius.

Scattered light observations trace the illumination of the small grains in the disk. Like the  $^{12}\text{CO}$  line, scattered light trace the upper layers of the disk, and is thus worth comparing the two. The scattered light image of AS 209 presented recently by Avenhaus et al. (2018) was found to be very faint and feature-less in comparison to other disks of similar mass. Although the emission is faint, it is detected up to 200 au. The faint nature of the disk could be the result of shadowing of the outer disk by one of the rings in the inner disk, most likely the one near 15 au. Another possibility is that the disk has experienced substantial settling and it is thus very flat. From these observations, the authors also computed the deprojected profiles for two possible scenarios in which



**Figure 5.** Moment-zero map (upper) and azimuthally-averaged deprojected radial profile (bottom) of the  $^{12}\text{CO}$  2 – 1 line emission. Emission with signal-to-noise ratio lower than 3 has been clipped. Only the uncontaminated East part of the image was considered to create the deprojected profile. The four vertical bars mark the position of the CO gaps. The two white (black in lower panel) dotted lines mark the position of the prominent outer dust rings, located at 75 and 120 au, and the green dotted line marks the position of the outermost CO gap near 210 au.

the North and the South part of the disk are closer to us. The new CO observations suggest the latter alternative is the correct one (see discussion below for the orientation of the disk). For this scenario, the resulting radial profile of the scattered light emission presents three rings, two of them located near the dust rings seen by ALMA, and a third one near 250 au. They also find a

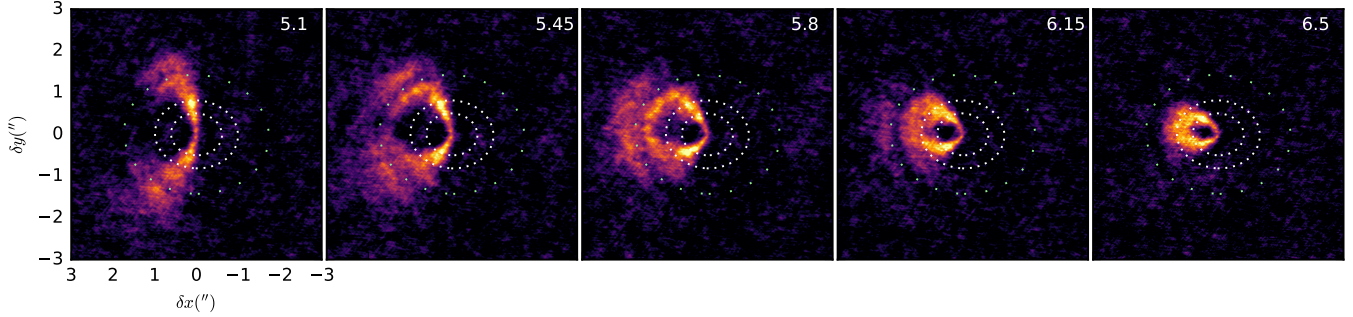


**Figure 6.** Channel-maps of the  $^{12}\text{CO}$  2 – 1 line emission. Only channels from the uncontaminated East side of the disk are shown. The velocity of each channel is shown in top right corner. The two inner ellipses (dotted lines) mark the position of the two brighter outer dust rings located at 74 and 120 au. A third ellipse (green dotted line) corresponding to a projected radius of 210 au is also drawn, to mark the position of a gap of CO emission in the outer disk.

gap near 200 au. This outer ring and gap coincide with the gap and outer ring seen in the CO emission.

These high-angular resolution observations of the CO line allows us to determine the orientation of the disk (Rosenfeld et al. 2013). Because the CO line is optically thick and the disk is flared, the observed emission originates from the surface layers of the disk which are elevated with respect to the midplane, where the dust continuum emission arises. At enough angular resolution and if the disk is inclined enough, it is thus possible to differentiate the front and back side of the disk. In the case of AS 209, the south part of the disk appear to be closer to us. Indeed, the half-disk that is closer to us and appears brighter in the channel maps, is shifted to the north, and the half-disk that is pointing to the back appears dimmer and is shifted to the south. This effect is better seen at velocities of  $5.8$  and  $6.1 \text{ km s}^{-1}$ . The separation of the back and front sides of the disk is much clearer for other disks, like IM Lup (Huang et al. 2018b) and HD 163296 (Isella et al. 2018). Both these disks are more inclined than AS 209, which could explain the difference.

#### 4. DISCUSSION

Although other disks (excluding disks with large inner cavities) are known to harbor multiple rings and gaps in their millimeter emission, namely HL Tau (ALMA Partnership et al. 2015), TW Hya (Andrews et al. 2016) and HD 163296 (Isella et al. 2016) disks, the disk around the AS 209 star is very unique. This is because, although there is substantial substructure throughout the disk that can be fully explained with concentric axisymmetric Gaussian rings, there is a striking difference between the inner and outer disk. While the inner disk consists of close-by rings which resemble the emission seen in TW Hya and HD 163296, the outer disks harbors two prominent rings that are separated by a gap with a much higher contrast compared to the other disks [Is this true in the case of HD163296? what is the contrast there?]. In this section we discuss the

different possible origins for these substructures, in both the dust continuum and the CO line emission.

##### 4.1. Origin of the dust emission ring-morphology

One of the main results from the DSHARP Large Program is that rings and gaps are very common in full protoplanetary disks (Huang et al. 2018a), but the origin of these substructures is still unknown. Several alternatives have been proposed, the most popular being the presence of planets. An embedded planet can induce a gap opening (or multiple gaps) by dynamic interactions with the disk. In principle, the gap width will depend on the mass of the planet – more massive planets opening wider gaps (e.g., Rosotti et al. 2016). The depth of the gap will depend on several factors, including the mass of the planet, the time the planet has had to carve the gap, the disk aspect ratio  $h/r$ , and the disk viscosity – planets will open deeper gaps in low viscosity disks (e.g. Crida et al. 2006; Dong & Fung 2017; Bae et al. 2017). Using 3D hydro-dynamical simulations, Fedele et al. (2018) found that the outer gap position, width and depth of the outermost gap is consistent with the presence of a  $0.2 M_J$  planet located at 95 au. The same planet could produce the other prominent gap seen in the continuum at 60 au. Another possibility, also consistent with the observations, is the presence of a second  $\sim 0.1 M_J$  planet in the inner gap at 57 au, close to a 2:1 resonance with the outer planet. In either case, the presence of a planet at such a large radius of 95 au, that would have formed within  $< 2$  Myr and then opened a gap, challenges our current understanding of planet formation by core accretion.

The higher-angular resolution observations reveal the presence of additional gaps, or dark annulus in the inner disk, that were unresolved in the  $\sim 0.16''$  resolution observations of Fedele et al. (2018). They did, however, detect a kink near  $20 - 30$  au, which we now know corresponds to the presence of four rings in the inner disk. The multiple rings seen in the inner disk could also be produced by planets in the outer disk. Simulations by Bae et al. (2017) showed that a single  $30 M_{\text{Earth}}$  planet

could produce major gaps both interior of the planet location and in the outer disk. A particular new feature in the AS 209 disk is the dark annuli at roughly 10 au. The gap is not as deep as the gaps in the outer disk, and it is not seen in the scattered light image, probably because it is hidden by the 0.185'' coronagraph (Avenhaus et al. 2018). New simulations show that a single planet located near 100 au could produce simultaneously the various rings seen in the inner  $< 60$  au and outer disk in AS 209 (Zhu et al. 2018). **Do we show the radial profile of the best simulation? what is the mass of the planet? [Zhaohuan?].**

It is worth to note that the most prominent gaps seen in the dust continuum are not seen as prominent features in the CO emission (but see section 4.2). This does not discard the planet alternative, as theoretical simulations have shown that it is possible for planets to open gaps in the dust while leaving the gas emission relatively featureless (Dipierro & Laibe 2017), specially for optically thin lines like  $^{12}\text{CO}$ . This is particularly true if the planet has a low mass, which is the case for the putative planets in AS 209 (Fedele et al. 2018).

It has also been suggested that the rings observed at millimeter wavelengths could be produced by changes in the dust properties at the location of snowlines of the main ices, like  $\text{H}_2\text{O}$ ,  $\text{NH}_3$ ,  $\text{CO}$  and  $\text{N}_2$  (Zhang et al. 2015). In this scenario, at the location of the condensation fronts material can be concentrated which is critical for the formation of planetesimals. At these locations the  $\mu\text{m}$ -sized and mm-sized dust particles would have grown to cm sizes and larger, and would thus be invisible at millimeter wavelengths, appearing as gaps in the observations. We can estimate the location of these snowlines in the AS 209 disk, using the midplane temperature derived by Andrews et al. (2009) (see also, Huang et al. 2016). The two outer gaps in the disk, near 60 and 100 au, have temperatures of 20 and 15 K, which are comparable to the condensation temperatures of pure CO and  $\text{N}_2$  ices, respectively (Zhang et al. 2015). The water snowline, which is supposed to be the most efficient snowline to concentrate solids, is located very close to the central star ( $< 2$  au), and is thus unresolved even with the ALMA observations. It is worth remembering that gas temperatures in disks are very uncertain. In particular, for the AS 209 disk the gas temperature was derived by fitting a power-law to lower angular resolution observations of the dust continuum (Andrews et al. 2009). The location of snowlines could therefore be shifted in the disk. A major problem with this scenario is that the gaps in the AS 209 disk are very wide (almost 20 au for the outermost gap) and also very depleted in dust. Although they may contribute some in the formation of these gaps, it is hard to explain how condensation fronts alone could produce such wide gaps.

Another alternative are zonal flows produced by MHD turbulence in the disk, which require large scale variations in the magnetic field (Johansen et al. 2009; Flock

et al. 2015; Béthune et al. 2016). Simulations of this effect predict radial variations of a few scale heights, which was found to be consistent for the case of the disk around TW Hya (Andrews et al. 2016), at least in the outer disk. In contrast to TW Hya, the rings in AS 209 are well separated by 1-20 au in the inner 60 au, and by 46 au in the outer disk. The gas scale height at these radii, however, are only 1 – 3 au and 5 – 10 au for the inner and outer disk, respectively (given the disk structure derived by Andrews et al. 2009). The contrast of the rings is also much larger than those observed towards TW Hya. This makes the magnetic alternative to be the cause of the ring-like structure much less likely. **I actually have no idea if this is true! help is welcomed for this alternative**

#### 4.2. Origin of the CO emission rings and gaps

One way to produce gaps in the CO emission is by optically thick dust emission. For a long time, dust opacity at millimeter wavelengths has thought to be negligible, at least in the outer disk. This is due to the low surface dust brightness temperature found in disks (of about 6–10 K), which are too low to produce absorption of the lines. However, recent high-angular resolution observations cast doubt on this assumption (see also the case of HD 163296; Isella et al. 2018). In the case of AS 209, the peak brightness temperature of the two prominent outer rings is  $\sim 0.15$ – $0.20$  mJy, which correspond to  $\sim 3$ – $4$  K, and would only produce an opacity of  $\sim 0.4$ – $0.5$  assuming a dust temperature of  $\sim 12$ – $15$  K (see also Dullemond et al. 2018). Nevertheless, the CO observations display a decrease of emission very close to location of these two dust rings, suggesting the dust rings are optically thick. One way to reconcile this problem is if the rings are not resolved and are clumpy in nature. A filling factor of 1/3 would be enough to reproduce the ratio between the dust temperature and the brightness temperature of the rings.

Huang et al. (2016) presented CO isotopologue observations of the AS 209 disk at 0.6'' angular resolution, and found that the  $\text{C}^{18}\text{O}$  emission consists of a central peak and a ring component centered at a radius of  $\sim 150$  au. Their optically thick  $^{12}\text{CO}$  emission, however, was found to be centrally peaked. The new higher angular resolution  $^{12}\text{CO}$  observations reveal some new interesting substructure. In particular, we detect a fainter outer ring centered at  $\sim 240$  au, which was not detected in the  $\text{C}^{18}\text{O}$  emission probably due to the lower signal-to-noise of the emission in the outer disk. The CO emission thus presents at least 2 ring components located outside the millimeter dust disk and also well outside the expected location of the CO snowline (between 30 and 90 au; Huang et al. 2016). Huang et al. (2016) suggested that the CO ring at 150 au is caused by CO being desorbed back into the gas-phase, which could happen by some non-thermal process (cosmic-rays or high-energy photons), or by thermal inversion due to dust migration.

However, the presence of a second ring at 240 au cast doubt on this interpretation. If chemistry is the cause of the outermost CO ring, then the inner ring should be produced by a different mechanism. Another alternative is that the outermost gap near 210 au corresponds to a reduction of the total gas density at this location. The fact that we can see this gap in the optically thick  $^{12}\text{CO}$  line suggest the the gas is depleted at all disk heights and not only in the midplane. The origin of this gap is unclear, but we can speculate it is produced by a planet. The formation of planets this far from the star are hard to explain theoretically, but indirect evidence of their existence has been found. Pinte et al. (2018) found localized deviation from Keplerian velocities in the CO emission, and attributed the observed velocity kink to a planet located  $\sim 260$  au from the young HD 163296 star. We do not detect any clear evidence of deviations from Keplerian velocities in the AS 209 disk, but this could be due to lower signal-to-noise ratio compared to the HD 163296 observations. Alternatively, the velocity kink could be present in the West side of the disk and thus hidden by the cloud contamination. We do not detect any localized emission at this radii in the dust continuum image either.

## 5. SUMMARY

We have presented observations of the 1.2 mm dust continuum and the  $^{12}\text{CO}$  2 – 1 line emission from the disk around the classical AS 209 star, as part of the ALMA Large Program DSHARP. We have modeled the dust emission in the uv-plane and find that the emission can be well-represented by a series of concentric rings. We find four rings in the inner  $< 60$  au disk, and two prominent rings in the outer disk, near 74 and 120 au, which were previously reported by Fedele et al. (2018). Two main gaps are seen, near 60 and 100 au. The second

gap at 100 au is not completely empty from mm-sized dust grains, however, as we detect faint dust emission within the gap. We also detect faint emission in the outer edge of the disk, out to  $\sim 160$  au. The CO also displays four gaps. Two of them spatially coincide with the position of the two prominent outer dust rings, which suggest the rings are optically thick. The outermost CO gap near  $\sim 210$  au is located well-beyond the millimeter dust edge, and therefore traces real CO depletion or a substantial decrease in the gas density.

We discuss the different possibilities for the origin of the gaps seen in the continuum emission. We find that the chemical alternative, that is snowline-induced gaps, is not very favored in this disk because the gap near 100 is too wide. A single planet of  $X M_J$  near 100 au could, however, produce the various rings seen in the continuum image, both in the inner disk and in the outer disk. If the presence of this planet is confirmed, then planet formation starts very early (few Myr) in the evolution of disks. Moreover, the presence of planets at such large distance from the central star challenge our current understanding of the planet formation process.

V.V.G. and J.C acknowledge support from the National Aeronautics and Space Administration under grant No. 15XRP15\_20140 issued through the Exoplanets Research Program. This paper makes use of the following ALMA data: ADS/JAO.ALMA# 2016.1.00484.L, ADS/JAO.ALMA# 2013.1.00226 and ADS/JAO.ALMA# 2015.1.00486.S. ALMA is a partnership of ESO (representing its member states), NSF (USA) and NINS (Japan), together with NRC (Canada), NSC and ASIAA (Taiwan), and KASI (Republic of Korea), in cooperation with the Republic of Chile. The Joint ALMA Observatory is operated by ESO, AUI/NRAO and NAOJ.

## REFERENCES

- ALMA Partnership, Brogan, C. L., Pérez, L. M., et al. 2015, ApJL, 808, L3
- Andrews, S. M., Wilner, D. J., Hughes, A. M., Qi, C., & Dullemond, C. P. 2009, ApJ, 700, 1502
- Andrews, S. M., Wilner, D. J., Zhu, Z., et al. 2016, ApJL, 820, L40
- Andrews, et al. 2018, ApJL,
- Avenhaus, H., Quanz, S. P., Garufi, A., et al. 2018, arXiv:1803.10882
- Bae, J., Zhu, Z., & Hartmann, L. 2017, ApJ, 850, 201
- Béthune, W., Lesur, G., & Ferreira, J. 2016, A&A, 589, A87
- Cieza, L. A., Casassus, S., Pérez, S., et al. 2017, ApJL, 851, L23
- Crida, A., Morbidelli, A., & Masset, F. 2006, Icarus, 181, 587
- Dipierro, G., & Laibe, G. 2017, MNRAS, 469, 1932
- Dong, R., & Fung, J. 2017, ApJ, 835, 146
- Dullemond, K., et al. 2018, ApJ,
- Fedele, D., Tazzari, M., Booth, R., et al. 2018, A&A, 610, A24
- Flock, M., Ruge, J. P., Dzyurkevich, N., et al. 2015, A&A, 574, A68
- Foreman-Mackey, D., Conley, A., Meierjürgen Farr, W., et al. 2013, Astrophysics Source Code Library, ascl:1303.002
- Gaia Collaboration, Brown, A. G. A., Vallenari, A., et al. 2018, arXiv:1804.09365

- Herbig, G. H., & Bell, K. R. 1988, Third catalog of emission-line stars of the Orion population., by G.H. herbig and K.R. Bell. Lick Observatory Bulletin #1111, Santa Cruz: Lick Observatory, Jun 1988, 90 p., 1111
- Huang, J., Öberg, K. I., & Andrews, S. M. 2016, ApJL, 823, L18
- Huang, J., et al. 2018, Rings ApJL,
- Huang, J., et al. 2018, Spirals ApJL,
- Isella, A., Guidi, G., Testi, L., et al. 2016, Physical Review Letters, 117, 251101
- Isella, A., et al. 2018,
- Johansen, A., Youdin, A., & Klahr, H. 2009, ApJ, 697, 1269
- Öberg, K. I., Murray-Clay, R., & Bergin, E. A. 2011, ApJL, 743, L16
- Pearson, T. J. 1999, Synthesis Imaging in Radio Astronomy II, 180, 335
- Pérez, L. M., Carpenter, J. M., Chandler, C. J., et al. 2012, ApJL, 760, L17
- Pinte, C., Price, D. J., Ménard, F., et al. 2018, ApJL, 860, L13
- Pinilla, P., Birnstiel, T., Ricci, L., et al. 2012, A&A, 538, A114
- Rosenfeld, K. A., Andrews, S. M., Hughes, A. M., Wilner, D. J., & Qi, C. 2013, ApJ, 774, 16
- Rosotti, G. P., Juhasz, A., Booth, R. A., & Clarke, C. J. 2016, MNRAS, 459, 2790
- Tazzari, M., Testi, L., Ercolano, B., et al. 2016, A&A, 588, A53
- Zhang, K., Blake, G. A., & Bergin, E. A. 2015, ApJL, 806, L7
- Zhu, Z. et. al. 2018,

## APPENDIX

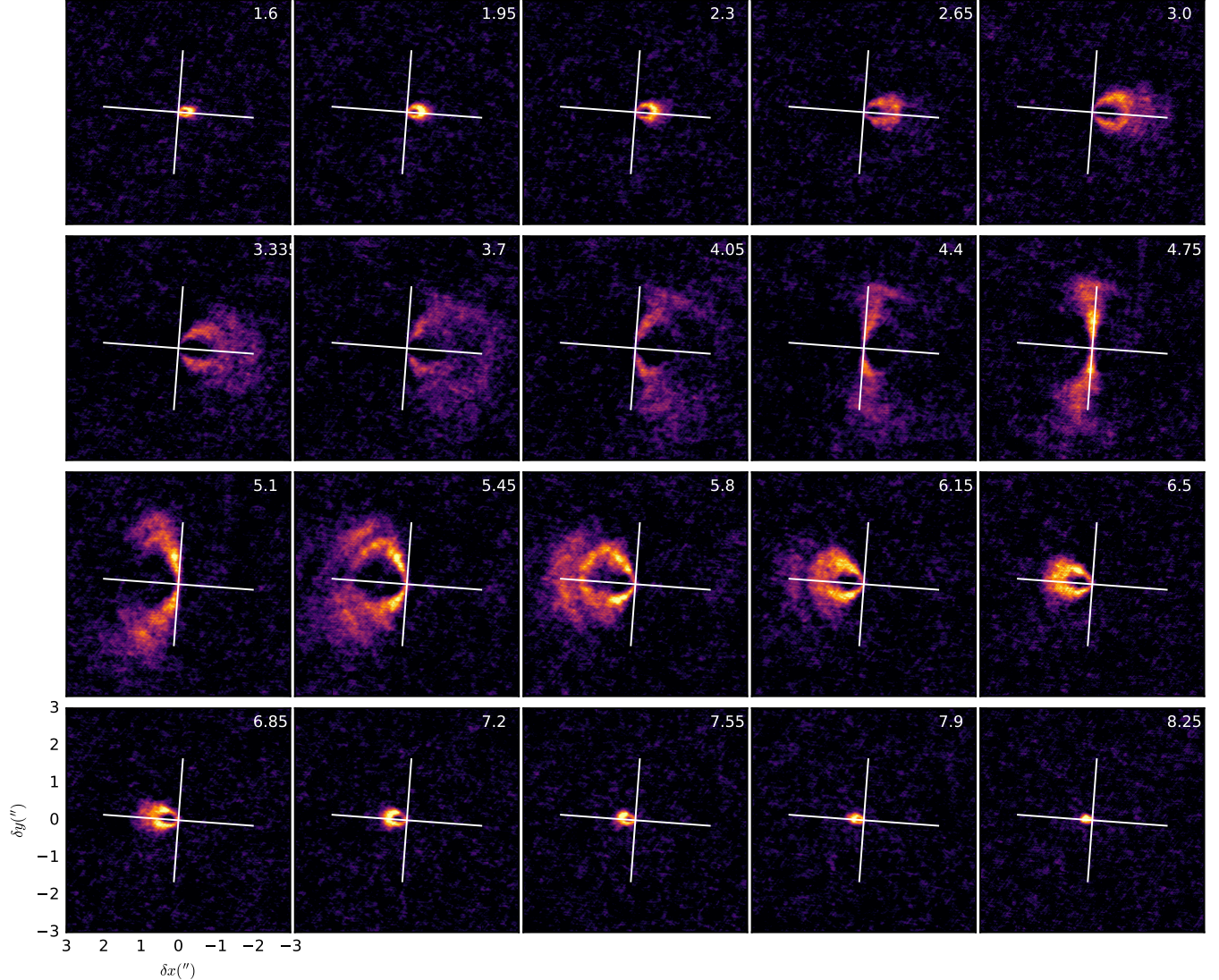


**Figure 7.** Channel-maps of the  $^{12}\text{CO}$  2 – 1 line emission. The velocity of each channel is shown in top right corner. The major and minor axis are shown in white.